Dalton Transactions

Accepted Manuscript

ROYAL SOCIETY OF CHEMISTRY

www.rsc.org/dalton

Quaternary chalcogenides Ba$RE_2In_2Ch_7$ (RE = La–Nd; Ch = S, Se) containing InCh_5 trigonal bipyramids†

Wenlong Yin,[a,b] Abishek K. Iyer,[a] Xinsong Lin,[c] Chao Li,[d] Jiyong Yao,[d] and Arthur Mar*[a]

[a] *Department of Chemistry, University of Alberta, Edmonton, Alberta, Canada T6G 2G2*

[b] *Institute of Chemical Materials, China Academy of Engineering Physics, Mianyang 621900 People's Republic of China*

[c] *Centre for Oil Sands Sustainability, Northern Alberta Institute of Technology, Edmonton, Alberta, Canada T6N 1E5*

[d] *Center for Crystal Research and Development, Technical Institute of Physics and Chemistry, Chinese Academy of Sciences, Beijing 100190, People's Republic of China*

* *Department of Chemistry, University of Alberta, Edmonton, Alberta, Canada T6G 2G2. E-mail: arthur.mar@ualberta.ca; Fax: +1-780-492-8231*

† Electronic supplementary information (ESI) available: EDX analyses, powder XRD patterns, and additional band structure results. See DOI: 10.1039/xxxxxxxx

Abstract

Eight new quaternary chalcogenides Ba$RE_2In_2Ch_7$ (RE = La–Nd; Ch = S, Se) have been prepared by reactions of BaCh, In_2Ch_3, RE, and Ch at high temperatures. They adopt orthorhombic structures (space group *Pbam*, Z = 2; a = 11.6300(8)–11.5895(7) Å, b = 12.4202(9)–12.3001(8) Å, c = 4.0689(3)–4.0028(2) Å for the sulfides; a = 12.1515(6)–12.1358(10) Å, b = 12.9367(7)–12.8510(11) Å, c = 4.1966(2)–4.1363(4) Å for the selenides) containing one-dimensional anionic [In_2Ch_7] ribbons of corner-sharing InCh_5 trigonal bipyramids, separated by Ba and RE cations. The structure is an ordered variant of the rare $Eu_3Sn_2S_7$-type with Ba atoms occupying larger sites with nearly cubic geometry and RE atoms occupying smaller sites with bicapped trigonal prismatic geometry. The InCh_5 trigonal bipyramids, which are unusual, exhibit four shorter In–Ch bonds and a fifth longer one. Band structure calculations indicate that $BaLa_2In_2S_7$ is a direct gap semiconductor, and corroborate the description of the In coordination as CN4+1. On the basis of optical absorption spectra, band gaps were estimated to be 1.87(2) eV for $BaLa_2In_2S_7$ and 1.66(2) eV for $BaLa_2In_2Se_7$.

Keywords: Chalcogenides; Rare earths; Crystal structure; Electronic structure; Optical properties

Introduction

Quaternary chalcogenides *A*–*RE*–*M*–*Ch* (where *A* = alkali or alkaline-earth metal; *RE* = rare-earth metal; *M* = d- or p-block metal or metalloid; *Ch* = S, Se, Te) exhibit considerable compositional and structural diversity arising from the nearly limitless ways of connecting coordination polyhedra.[1–5] They have provided many new candidates for materials applications resulting from several attractive features: they are usually semiconductors whose band gaps can be modified by judicious control of composition, they often contain magnetically active species in complex arrangements, and they are typically air-stable and thermodynamically robust. Some notable past examples include $Cs_xRE_2Cu_{6-x}Te_6$ as thermoelectric materials,[6] $AREMCh_3$ (*A* = Rb, Cs; *M* = divalent transition metals) as semiconductors with variable band gaps,[7–11] and $BaRE_2MS_5$ (*M* = Mn–Co) as antiferromagnets.[12–16]

Until recently, the systems *A*–*RE*–*M*–*Ch* (*A* = alkaline-earth metal; *M* = Ga, In) were poorly investigated. The few quaternary chalcogenides known in these systems were $ARE Ga_3S_7$ (*A* = Ca, Sr; *RE* = La, Ce),[17,18] $A_{1-x}Eu_xGa_2S_4$ (*A* = Sr, Ba),[19,20] and $CaYbInCh_4$ (*Ch* = S, Se),[21] with only the latter having ordered structures. Renewed efforts have led to the identification of many more compounds. Most of these compounds belong to five series having the same composition but adopting three different structure types containing Ga- or In-centred tetrahedra: Ba_2REGaS_5 ($I4/mcm$),[22] $Ba_2REGaSe_5$ ($P\bar{1}$),[23] $Ba_2REGaTe_5$ ($P\bar{1}$ and $Cmc2_1$),[24] $Ba_2REInSe_5$ ($Cmc2_1$),[23,25] and $Ba_2REInTe_5$ ($Cmc2_1$).[24] A sixth series is Ba_3REInS_6 ($R\bar{3}c$), whose structure contains In-centred octahedra.[22] Among these compounds, Ba_2YInSe_5 exhibits a strong second harmonic generation (SHG) response close to that of $AgGaSe_2$,[23] and Ba_2YInTe_5 is predicted to be a potentially good thermoelectric material.[26]

In continuation of these efforts, we report here the new series of quaternary chalcogenides Ba$RE_2In_2Ch_7$ (*RE* = La–Nd; *Ch* = S, Se) and the characterization of their crystal and electronic structures. We discuss structural relationships and examine the interesting coordination environment of the In atoms in these compounds.

Experimental

Synthesis

Ba rods (99%, Alfa-Aesar), freshly filed *RE* pieces (99.9%, Hefa), In powder (99.99%, Sigma-Aldrich), S flakes (99.998%, Sigma-Aldrich), Se powder (99.99%, Sigma-Aldrich), and BaS powder (99%, Alfa-Aesar) were used as obtained. Binary starting materials BaSe, In_2S_3, and In_2Se_3 were prepared by stoichiometric reaction of the elements at high temperatures (1173 K for BaSe, 1273 K for In_2S_3, and 873 K for In_2Se_3) in sealed fused-silica tubes.

Exploratory syntheses were initially carried out in the Ba–La–In–S system. The starting materials BaS, La, In_2S_3, and S were combined in the appropriate molar ratios to target the loading compositions $BaLaInS_4$, $BaLaIn_3S_7$, $BaLa_3InS_7$, and $BaLa_2In_2S_7$, each with a total mass of 0.3 g. The mixtures were pressed into pellets, loaded into fused-silica tubes which were evacuated and sealed, and placed into a computer-controlled furnace. The tubes were heated to 1323 K over 30 h, held at this temperature for 72 h, cooled slowly to 973 K over 96 h, cooled to 873 K over 24 h, and then cooled to room temperature over 24 h. Small black needle-shaped crystals were obtained in low yield from the reactions with loading compositions $BaLaInS_4$ and $BaLaIn_3S_7$. These crystals were examined on a JEOL JSM-6010 LA scanning electron microscope and found by energy-dispersive X-ray (EDX) analysis to have the composition $BaLa_2In_2S_7$, as subsequently established by the structure determination. Attempts were made to

substitute La with all other feasible trivalent *RE* metals (from Ce to Lu), using analogous loading compositions and temperature profiles as above. As confirmed by EDX analyses, crystals of Ba$RE_2In_2S_7$ were obtained only for *RE* = Ce, Pr, and Nd from the reactions with loading compositions Ba*RE*InS_4 and Ba*RE*In_3S_7. For other *RE* substitutions (*RE* = Sm, Gd–Lu), the desired Ba$RE_2In_2S_7$ phase was not obtained under similar conditions. The reactions were extended to prepare the selenides using analogous loading compositions as before but with the temperature profile modified slightly so that the first step involves heating to 1273 K (instead of 1323 K) and with *RE* substitutions attempted for La–Dy. Crystals of Ba$RE_2In_2Se_7$ were obtained from reactions with loading compositions Ba*RE*In_3Se_7 for *RE* = La–Nd. Crystals of all Ba$RE_2In_2Ch_7$ compounds are stable in air for months. EDX analyses of these crystals agreed well with expectations (Table S1 in ESI†).

Polycrystalline samples of Ba$RE_2In_2Ch_7$ (*RE* = La–Nd; *Ch* = S, Se) were prepared by stoichiometric reaction of Ba*Ch*, *RE*, In_2Ch_3, and *Ch* in the molar ratio of 1:2:1:3. The mixtures were heated to 1073 K over 24 h and kept there for 48 h, after which the furnace was turned off. The samples were reground, loaded into new tubes, and reheated at 1073 K for 72 h. Powder X-ray diffraction (XRD) patterns were collected on an Inel diffractometer equipped with a curved position-sensitive detector (CPS 120) and a Cu $K\alpha_1$ radiation source operated at 40 kV and 20 mA (Fig. S1 in ESI†). The samples contained the desired quaternary chalcogenides with varying amounts of $BaIn_2S_4$ or $BaIn_2Se_4$ as a byproduct.

Structure determination

Single crystals of high quality and suitable size were available for the entire series Ba$RE_2In_2Ch_7$ (*RE* = La–Nd; *Ch* = S, Se). Intensity data were collcted at room temperature on a Bruker

PLATFORM diffractometer equipped with a SMART APEX II CCD area detector and a graphite-monochromated Mo *K*α radiation source, using ω scans at 5–8 different ϕ angles with a frame width of 0.3º and an exposure time of 15–20 s per frame. Face-indexed numerical absorption corrections were applied. Structure solution and refinement were carried out with use of the SHELXTL (version 6.12) program package.[27] The centrosymmetric orthorhombic space group *Pbam* was chosen on the basis of Laue symmetry and intensity statistics. Initial locations of all atoms were found by direct methods. The structure refinements for all compounds were straightforward, leading to excellent agreement factors (with conventional $R(F)$ values of 0.03–0.04) and featureless difference electron density maps (with $(\Delta\rho)_{max}$, $(\Delta\rho)_{min}$ values generally around 3 and –3 e/Å^3, respectively). All atoms had reasonable displacement parameters and were confirmed to be fully occupied. Atom positions and labels were standardized with the program STRUCTURE TIDY.[28] Crystal data and further details are listed in Table 1, positional and equivalent isotropic displacement parameters in Table 2, and interatomic distances in Table 3. Further data, in CIF format, have been sent to Fachinformationszentrum Karlsruhe, Abt. PROKA, 76344 Eggenstein-Leopoldshafen, Germany, as supplementary material No. CSD-431403 to 431410 and can be obtained by contacting FIZ (quoting the article details and the corresponding CSD numbers).

Diffuse reflectance spectroscopy

A compacted pellet of $BaSO_4$ was used as a 100% reflectance standard. Spectra for $BaLa_2In_2S_7$ and $BaLa_2In_2Se_7$ were collected from 300 nm (4.13 eV) to 2500 nm (0.50 eV) on a Cary 5000 UV-vis-NIR spectrophotometer equipped with a diffuse reflectance accessory. Optical absorption spectra were converted from the diffuse reflectance spectra using the Kubelka-Munk

function, $F(R) = \alpha/S = (1–R)^2/2R$, where α is the Kubelka-Munk absorption coefficient, S is the scattering coefficient, and R is the reflectance.[29]

Band structure calculations

Tight-binding linear muffin tin orbital band structure calculations on $BaLa_2In_2S_7$ and $BaLa_2In_2Se_7$ were performed within the local density and atomic spheres approximation with use of the Stuttgart TB-LMTO-ASA program (version 4.7).[30] The basis set consisted of Ba 6s/(6p)/5d/(4f), La 6s/(6p)/5d/(4f), In 5s/5p/(5d), and S 3s/3p/(3d) or Se 4s/4p/(4d) orbitals, with the orbitals shown in parentheses being downfolded. Integrations in reciprocal space were carried out with an improved tetrahedron method over 63 irreducible k points within the first Brillouin zone.

Results and discussion

The quaternary chalcogenides Ba$RE_2In_2Ch_7$ (RE = La–Nd; Ch = S, Se) were obtained from high-temperature reactions of BaCh, RE, In_2Ch_3, and Ch. It was difficult to avoid formation of $BaIn_2Ch_4$ in polycrystalline samples prepared from reactions at 1073 K, even after regrinding and reheating; the best results were found for the La-containing samples, which contained ~5% of $BaIn_2Ch_4$. These compounds represent new series of quaternary chalcogenides found in the A–RE–In–(S, Se) systems (where A = alkaline-earth metal), in which $Ba_3RE InS_6$ (RE = Pr, Sm, Gd, Yb),[22] $Ba_2RE InSe_5$ (RE = Y, Nd, Sm, Gd, Dy, Er, Yb),[23,25] and CaYbInCh_4 (Ch = S, Se)[21] were previously known.

These chalcogenides adopt a new orthorhombic structure type (in space group *Pbam*) which can be considered to be an ordered variant of the $Eu_3Sn_2S_7$-type,[31] an exceedingly rare one

that has been found for only three examples ($Eu_3Sn_2S_7$,[31,32] $Sr_3Sn_2S_7$,[33] and $Tl_3Cd_2I_7$ [34]). The unit cell volumes decrease quite regularly on proceeding from La to Nd for the *RE* component within both the sulfide and selenide series, in accordance with the lanthanide contraction (Fig. 1). For concreteness, we choose $BaLa_2In_2S_7$ to describe the structure and arbitrarily designate this member as the name of the structure type. The structure consists of one-dimensional arrangements of anionic [In_2S_7] ribbons which extend down the *c*-direction and are separated by Ba and La cations (Fig. 2). The local coordination geometries formed by the S atoms around the metal atoms are highly regular (Fig. 3). The Ba atoms are centred within a slightly distorted cube (properly, a rectangular prism), with nearly equal Ba–S distances (3.2986(11)–3.2997(11) Å). Although eight-coordination is common for Ba atoms in many complex chalcogenides, cubic geometry is not typical. A high-pressure form of BaS (with CsCl-type structure) exhibits Ba in cubic geometry;[35] BaS_3 contains Ba in cuboctahedral coordination (CN12) but if the four longer distances are neglected, then a cubic geometry is obtained.[36] The La atoms are also eight-coordinate but are centred within a bicapped trigonal prism, which is frequently observed, having shorter distances to the S atoms (2.8933(10)–3.2956(16) Å). The In atoms are five-coordinate and centred within a trigonal bipyramid, which is unusual. The distances from In to the three equatorial and one of the apical S atoms are short (2.4576(15)–2.5449(15) Å); the fifth distance to the remaining apical S atom is considerably longer (2.8979(5) Å). Thus it will be of interest to determine whether the fifth In–S distance is truly bonding and whether the coordination is more properly described as CN4+1. The same observation of a fifth longer distance applies to the In atoms within the corresponding quaternary selenides. In other In-containing chalcogenides, tetrahedral (CN4) and octahedral (CN6) coordination geometries are normally found around In

atoms;[23–26] in contrast, examples of trigonal bipyramidal (CN5) geometry are few, being found in γ-In_2Se_3,[37,38] $AlInS_3$,[39] and $GaInS_3$.[40]

The In-centred trigonal bipyramids are connected in an interesting way. Pairs of InS_5 polyhedra are bridged by a common S4 atom to form In_2S_9 dimers, which then share corners, through the S1 atoms above and below along the *c*-direction, to form infinite double chains or ribbons with the formulation $[In_2S_5S_{4/2}]$, or $[In_2S_7]$. These one-dimensional ribbons are linked along the *a*-direction by the Ba atoms and along the *b*-direction by the La atoms to give the three-dimensional framework. This connectivity is quite different than found in the structures of other quaternary chalcogenides in the Ba–*RE*–*M*–*Ch* (*M* = Ga, In; *Ch* = S, Se) systems. More generally, the *M*-centred polyhedra are isolated, in the form of GaS_4 tetrahedra in Ba_2REGaS_5 (Cs_3CoCl_5-type),[22] $GaSe_4$ tetrahedra in $Ba_2REGaSe_5$ (Ba_2YGaSe_5-type),[23] and InS_6 octahedra in Ba_3REInS_6 ($K_3NaFeCl_6$-type).[22] An exception is $Ba_2REInSe_5$ (Ba_2BiInS_5-type), where $InSe_4$ tetrahedra share corners to form infinite chains.[23] As the *RE* component is changed in $BaRE_2In_2S_7$, the In_2S_9 dimers remain quite rigid, the bond lengths and angles varying little. Because the angle around the briding S4 atom is constrained by symmetry to be exactly 180°, the In_2S_9 dimer cannot distort by bending at this atom. Rather, the main effect is that the S1–In–S1 angle around the equatorial waist of each of the InS_5 trigonal bipyramids becomes slightly narrower (from 110.98(6)° in $BaLa_2In_2S_7$ to 109.28(6)° in $BaNd_2In_2S_7$), causing an overall compression of the $[In_2S_7]$ ribbons along *c* (which is the cell parameter that experiences the greatest contraction, by about 1.6%, upon substitution of the *RE* component). A less pronounced compression (with the Se1–In–Se1 angles decreasing from 108.41(3)° in $BaLa_2In_2Se_7$ to 106.97(5)° in $BaNd_2In_2Se_7$) is seen for the selenides $BaRE_2In_2Se_7$.

The quaternary chalcogenide $BaLa_2In_2S_7$ is easily derived from the ternary chalcogenide $Eu_3Sn_2S_7$ by comparing their charge-balanced formulations, $(Ba^{2+})(La^{3+})_2(In^{3+})_2(S^{2-})_7$ and $(Eu^{2+})_3(Sn^{4+})_2(S^{2-})_7$. To maintain charge neutrality, the aliovalent substitution of two Sn^{4+} cations in $Eu_3Sn_2S_7$ with two In^{3+} cations requires charge compensation as manifested by replacement of the electropositive divalent components with trivalent ones, to result in $BaLa_2In_2S_7$. Of the two Eu sites (both CN8) in $Eu_3Sn_2S_7$, the one in 2*d* having cubic coordination is slightly larger (with average Eu–S distance of 3.178 Å) than the one in 4*h* having bicapped trigonal prismatic coordination (with average Eu–S distance of 3.076 Å).[31] Correspondingly, in $BaLa_2In_2S_7$, the larger Ba atoms prefer the 2*d* site (with average Ba–S distance of 3.299 Å) while the smaller La atoms prefer the 4*h* site (with average La–S distance of 3.038 Å). The charge-balanced assignment is supported by calculations of bond valence sums[41] for all members of $BaRE_2In_2Ch_7$ (Table 4). These bond valence sums are 1.8–1.9 for the Ba atoms, 2.7–2.9 for the *RE* atoms, 3.0–3.2 for the In atoms, and 1.8–2.1 for the *Ch* atoms.

The electronic band structures were calculated for $BaLa_2In_2S_7$ and $BaLa_2In_2Se_7$; as the results are similar, only the former is discussed in detail here. The density of states (DOS) curve shows a gap of 1.55 eV between valence and conduction bands in $BaLa_2In_2S_7$ (Fig. 4a). Band dispersion curves (not shown here) indicate that $BaLa_2In_2S_7$ is a direct band gap semiconductor at the Brillouin zone centre (Γ). As confirmed by the atomic projections of the DOS curve, the more electropositive Ba and La atoms contribute mostly to empty states above the Fermi level while the more electronegative In and S atoms contribute mostly to filled states below. However, there is some interaction of Ba and La s-orbitals with S p-orbitals, giving rise to covalent contributions to Ba–S and La–S bonding, as seen in the crystal orbital Hamilton population (COHP) curves (Fig. 4b). These are non-negligible interactions, as gauged by the

integrated COHP (–ICOHP) values of 0.37 eV/bond (or 2.9 eV/cell) for Ba–S and 0.69 eV/bond (or 5.5 eV/cell) for La–S contacts. The S p-orbitals are also mixed with In s-orbitals (at –5.7 to –4.2 eV) and In p-orbitals (at –3.8 to 0 eV), resulting in strong bonding interactions within the InS_5 trigonal bipyramid. Close inspection of the COHP curves reveals a clear distinction between the four short In–S contacts, for which bonding is optimized with filling of all bonding and no antibonding levels, and the fifth longer one, for which antibonding levels involving overlap of In p and S p orbitals are found just below the Fermi level. Nevertheless, this long In–S bond cannot be dismissed, as its strength is about 28% (–ICOHP of 0.62 eV/bond) that of the other four In–S bonds (–ICOHP of 2.18 eV/bond). Analogous conclusions can be drawn for the selenide $BaLa_2In_2Se_7$, for which the calculated band gap is smaller (0.92 eV) and the fifth long In–Se bond is about 25% (–ICOHP of 0.51 eV/bond) as strong as the other four In–Se bonds (–ICOHP of 2.06 eV/bond) (Fig. S2 in ESI†). A correct description of the coordination around the In atoms in Ba$RE_2In_2Ch_7$ is thus CN4+1, as proposed above, and similarly for the Sn atoms in $Eu_3Sn_2S_7$ and $Sr_3Sn_2S_7$. In contrast, $Tl_3Cd_2I_7$ presents an interesting case where the fifth Cd–I bond is much longer (3.659 Å) than the other four (2.747–2.882 Å);[34] band structure calculations on this compound (not shown) indicate that this long bond is much weaker (–ICOHP of 0.18 eV/bond) than the other four bonds (–ICOHP of 1.80 eV/bond), so that CN4 is more appropriate here.

UV-vis-NIR diffuse reflectance spectra were obtained for $BaLa_2In_2S_7$ and $BaLa_2In_2Se_7$ (Fig. 5), which are predicted to be direct band gap semiconductors from the band structure calculations. The experimental optical band gaps, as deduced from plots of $(h\nu \cdot F(R))^2$ versus $h\nu$ through the straightforward extrapolation method,[42] were 1.87(2) eV for $BaLa_2In_2S_7$ and 1.66(2) eV for $BaLa_2In_2Se_7$, consistent with the black colour of these compounds.

Conclusions

The new chalcogenides Ba$RE_2In_2Ch_7$ further exemplify the potential richness of the quaternary Ba–*RE*–*M*–*Ch* (*M* = Ga, In; *Ch* = S, Se) systems and offered a new surprise in the form of an unusual motif of InCh_5 trigonal bipyramids, different from the more typical occurrence of tetrahedra (and less commonly, octahedra) in the previously known series. The relationship between the $BaLa_2In_2S_7$ and $Eu_3Sn_2S_7$ structure types illustrated here may serve as inspiration to target other substitutions that maintain the same electron count. Substitution of the electropositive components with combinations of alkali, alkaline-earth, or other rare-earth metals would seem likely.

Acknowledgements

This work was supported by the Natural Sciences and Engineering Research Council of Canada (through Discovery Grant no. 170209 and the ATUMS training program funded by the Collaborative Research and Training Experience Program) and the National Natural Science Foundation of China (No. 51402270 and 51132008).

References

1 P. Wu and J. A. Ibers, *J. Alloys Compd.*, 1995, **229**, 206–215.

2 K Mitchell and J. A. Ibers, *Chem. Rev.*, 2002, **102**, 1929–1952.

3 L. D. Gulay and M. Daszkiewicz, in *Handbook on the Physics and Chemistry of Rare Earths*, eds. K. A. Gschneidner, Jr., J.-C. G. Bünzli and V. K. Pecharsky, Elsevier, Amsterdam, 2011, pp. 157–273.

4 I. Chung and M. G. Kanatzidis, *Chem. Mater.*, 2014, **26**, 849–869.

5 J. Zhou, *Coord. Chem. Rev.*, 2016, **315**, 112–134.

6 C.-Y. Meng, H. Chen, P. Wang and L. Chen, *Chem. Mater.*, 2011, **23**, 4910–4919.

7 K. Mitchell, C. L. Haynes, A. D. McFarland, R. P. Van Duyne and J. A. Ibers, *Inorg. Chem.*, 2002, **41**, 1199–1204.

8 K. Mitchell, F. Q. Huang, A. D. McFarland, C. L. Haynes, R. C. Somers, R. P. Van Duyne and J. A. Ibers, *Inorg. Chem.*, 2003, **42**, 4109–4116.

9 K. Mitchell, F. Q. Huang, E. N. Caspi, A. D. McFarland, C. L. Haynes, R. C. Somers, J. D. Jorgensen, R. P. Van Duyne and J. A. Ibers, *Inorg. Chem.*, 2004, **43**, 1082–1089.

10 J. Yao, B. Deng, L. J. Sherry, A. D. McFarland, D. E. Ellis, R. P. Van Duyne and J. A. Ibers, *Inorg. Chem.*, 2004, **43**, 7735–7740.

11 G. H. Chan, L. J. Sherry, R. P. Van Duyne and J. A. Ibers, *Z. Anorg. Allg. Chem.*, 2007, **633**, 1343–1348.

12 H. Masuda, T. Fujino, N. Sato and K. Yamada, *J. Solid State Chem.*, 1999, **146**, 336–343.

13 M. Wakeshima and Y. Hinatsu, *J. Solid State Chem.*, 2000, **153**, 330–335.

14 M. Wakeshima, Y. Hinatsu, K. Oikawa, Y. Shimojo and Y. Morii, *J. Mater. Chem.*, 2000, **10**, 2183–2185.

15 M. Wakeshima and Y. Hinatsu, *J. Solid State Chem.*, 2001, **159**, 163–169.

16 K. Ino, M. Wakeshima and Y. Hinatsu, *Mater. Res. Bull.*, 2001, **36**, 2207–2213.

17 A.-M. Lozac'h, M. Guittard and J. Flahaut, *Mater. Res. Bull.*, 1973, **8**, 75–86.

18 A. B. Agaev, V. O. Aliev and O. M. Aliev, *Zh. Neorg. Khim.*, 1996, **41**, 319–325.

19 C. Hidaka and T. Takizawa, *J. Phys. Chem. Solids*, 2008, **69**, 358–361.

20 H. S. Yoo, W. B. Im, S. Vaidyanathan, B. J. Park and D. Y. Jeon, *J. Electrochem. Soc.*, 2008, **155**, J66–J70.

21 J. D. Carpenter and S.-J. Hwu, *Chem. Mater.*, 1992, **4**, 1368–1372.

22 K. Feng, Y. Shi, W. Yin, W. Wang, J. Yao and Y. Wu, *Inorg. Chem.*, 2012, **51**, 11144–11149.

23 W. Yin, K. Feng, W. Wang, Y. Shi, W. Hao, J. Yao and Y. Wu, *Inorg. Chem.*, 2012, **51**, 6860–6867.

24 W. Yin, W. Wang, L. Bai, K. Feng, Y. Shi, W. Hao, J. Yao and Y. Wu, *Inorg. Chem.*, 2012, **51**, 11736–11744.

25 K. Feng, W. Yin, W. Wang, L. Kang, W. Hao, J. Yao, Y. Shi, Z. Lin and Y. Wu, *Z. Anorg. Allg. Chem.*, 2013, **639**, 1021–1025.

26 W. Khan, S. Borek and J. Minar, *RSC Adv.*, 2015, **5**, 51461–51469.

27 G. M. Sheldrick, *SHELXTL, version 6.12*, Bruker AXS Inc., Madison, WI, 2001.

28 L. M. Gelato and E. Parthé, *J. Appl. Crystallogr.*, 1987, **20**, 139–143.

29 G. Kortüm, *Reflectance Spectroscopy*, Springer, New York, 1969.

30 R. Tank, O. Jepsen, A. Burkhardt and O. K. Andersen, *TB–LMTO–ASA Program, version 4.7*, Max Planck Institut für Festkörperforschung, Stuttgart, 1998.

31 S. Jaulmes and M. Julien-Pouzol, *Acta Crystallogr., Sect. B*, 1977, **33**, 3898–3901.

32 J. Flahaut, P. Laruelle, M. Guittard, S. Jaulmes, M. Julien-Pouzol and C. Lavenant, *J. Solid State Chem.*, 1979, **29**, 125–136.

33 M. Guittard, C. Lavenant and M. Palazzi, *C. R. Seances Acad. Sci., Ser. C*, 1978, **287**, 239–242.

34 V. V. Petrov, A. V. Bogdanova, E. K. Mashkarinets, V. K. Bel'skii, E. I. Gladyshevskii, I. R. Mokraya and V. K. Pecharskii, *Izv. Akad. Nauk SSSR, Neorg. Mater.*, 1987, **23**, 1395–1396.

35 S. Yamaoka, O. Shimomura, H. Nakazawa and O. Fukunaga, *Solid State Commun.*, 1980, **33**, 87–89.

36 S. Yamaoka, J. T. Lemley, J. M. Jenks and H. Steinfink, *Inorg. Chem.*, 1975, **14**, 129–131.

37 A. Likforman, D. Carré and R. Hillel, *Acta Crystallogr., Sect. B*, 1978, **34**, 1–5.

38 A. Pfitzner and H. D. Lutz, *J. Solid State Chem.*, 1996, **124**, 305–308.

39 M. Schulte-Kellinghaus and V. Krämer, *Acta Crystallogr., Sect. B*, 1979, **35**, 3016–3017.

40 G. G. Guseinov, I. R. Amiraslanov, A. S. Kuliev and Kh. S. Mamedov, *Izv. Akad. Nauk SSSR, Neorg. Mater.*, 1987, **23**, 854–856.

41 N. E. Brese and M. O'Keeffe, *Acta Crystallogr., Sect. B*, 1991, **47**, 192–197.

42 O. Schevciv and W. B. White, *Mater. Res. Bull.*, 1983, **18**, 1059–1068.

Table 1 Crystallographic data for Ba$RE_2In_2Ch_7$ (RE = La–Nd; Ch = S, Se)

	$BaLa_2In_2S_7$	$BaCe_2In_2S_7$	$BaPr_2In_2S_7$	$BaNd_2In_2S_7$
Formula mass (amu)	869.22	871.64	873.22	879.88
Space group	*Pbam* (No. 55)	*Pbam* (No. 55)	*Pbam* (No. 55)	*Pbam* (No. 55)
a (Å)	11.6300(8)	11.5947(7)	11.5920(6)	11.5895(7)
b (Å)	12.4202(9)	12.3439(8)	12.3232(7)	12.3001(8)
c (Å)	4.0689(3)	4.0413(3)	4.0210(2)	4.0028(2)
V (Å^3)	587.74(7)	578.41(7)	574.40(5)	570.61(6)
Z	2	2	2	2
ρ_{calcd} (g cm^{-3})	4.912	5.005	5.049	5.121
T (K)	296(2)	296(2)	296(2)	296(2)
Crystal dimensions (mm)	0.08 × 0.03 × 0.03	0.07 × 0.03 × 0.02	0.06 × 0.04 × 0.03	0.05 × 0.04 × 0.03
μ(Mo $K\alpha$) (mm^{-1})	15.46	16.19	16.86	17.54
Transmission factors	0.453–0.752	0.515–0.738	0.464–0.719	0.461–0.647
2θ limits	4.80–66.62°	4.82–66.58°	4.82–66.38°	4.83–66.55°
Data collected	$-17 \le h \le 17$, $-18 \le k \le 19$, $-6 \le l \le 6$	$-17 \le h \le 17$, $-18 \le k \le 19$, $-6 \le l \le 6$	$-17 \le h \le 17$, $-18 \le k \le 19$, $-6 \le l \le 6$	$-17 \le h \le 17$, $-18 \le k \le 18$, $-6 \le l \le 6$
No. of data collected	8324	8083	7994	8131
No. of unique data, including $F_o^2 < 0$	1261 (R_{int} = 0.052)	1239 (R_{int} = 0.060)	1228 (R_{int} = 0.060)	1228 (R_{int} = 0.046)
No. of unique data, with $F_o^2 > 2\sigma(F_o^2)$	1090	1022	1022	1061
No. of variables	40	39	39	40
$R(F)$ for $F_o^2 > 2\sigma(F_o^2)$ [a]	0.027	0.033	0.030	0.028
$R_w(F_o^2)$ [b]	0.058	0.075	0.063	0.062

Goodness of fit	1.104	1.127	1.141	1.186
$(\Delta\rho)_{max}$, $(\Delta\rho)_{min}$ (e Å^{-3})	1.91, –1.90	2.27, –1.89	2.21, –2.00	2.11, –1.91
	$BaLa_2In_2Se_7$	$BaCe_2In_2Se_7$	$BaPr_2In_2Se_7$	$BaNd_2In_2Se_7$
Formula mass (amu)	1197.52	1199.94	1201.52	1208.18
Space group	*Pbam* (No. 55)	*Pbam* (No. 55)	*Pbam* (No. 55)	*Pbam* (No. 55)
a (Å)	12.1515(6)	12.1364(7)	12.1433(8)	12.1358(10)
b (Å)	12.9367(7)	12.8927(8)	12.8798(9)	12.8510(11)
c (Å)	4.1966(2)	4.1741(3)	4.1547(3)	4.1363(4)
V (Å^3)	659.71(6)	653.13(7)	649.81(8)	645.09(10)
Z	2	2	2	2
ρ_{calcd} (g cm^{-3})	6.029	6.102	6.141	6.220
T (K)	296(2)	296(2)	296(2)	296(2)
Crystal dimensions (mm)	0.09 × 0.04 × 0.03	0.06 × 0.04 × 0.04	0.08 × 0.04 × 0.03	0.06 × 0.03 × 0.03
μ(Mo $K\alpha$) (mm^{-1})	31.98	32.73	33.39	34.13
Transmission factors	0.113–0.532	0.274–0.377	0.119–0.517	0.283–0.551
2θ limits	4.60–66.30°	4.61–66.50°	4.61–66.45°	4.62–66.49°
Data collected	$-18 \le h \le 18$, $-19 \le k \le 19$, $-6 \le l \le 6$	$-18 \le h \le 18$, $-19 \le k \le 19$, $-6 \le l \le 6$	$-18 \le h \le 18$, $-19 \le k \le 19$, $-6 \le l \le 6$	$-18 \le h \le 18$, $-19 \le k \le 19$, $-6 \le l \le 6$
No. of data collected	9266	9158	9108	9005
No. of unique data, including $F_o^2 < 0$	1407 (R_{int} = 0.053)	1403 (R_{int} = 0.054)	1392 (R_{int} = 0.059)	1391 (R_{int} = 0.089)
No. of unique data, with $F_o^2 > 2\sigma(F_o^2)$	1207	1195	1161	1062
No. of variables	40	40	40	39
$R(F)$ for $F_o^2 > 2\sigma(F_o^2)$ [a]	0.028	0.027	0.034	0.039

$R_w(F_o^2)$ [b]	0.060	0.059	0.077	0.085
Goodness of fit	1.144	1.148	1.136	1.119
$(\Delta\rho)_{max}$, $(\Delta\rho)_{min}$ (e Å^{-3})	1.72, –1.99	1.79, –2.33	4.52, –2.30	2.97, –2.43

[a] $R(F) = \sum||F_o| - |F_c|| / \sum|F_o|$ for $F_o^2 > 2\sigma(F_o^2)$. [b] $R_w(F_o^2) = [\sum[w(F_o^2 - F_c^2)^2] / \sum wF_o^4]^{1/2}$; $w^{-1} = [\sigma^2(F_o^2) + (Ap)^2 + Bp]$, where $p = [\max(F_o^2,0) + 2F_c^2] / 3$.

Table 2 Atomic coordinates and equivalent isotropic displacement parameters (Å^2) [a] for Ba$RE_2In_2Ch_7$ (RE = La–Nd; Ch = S, Se)

	$BaLa_2In_2S_7$	$BaCe_2In_2S_7$	$BaPr_2In_2S_7$	$BaNd_2In_2S_7$
Ba in 2*d* (0, ½, ½)				
U_{eq}	0.01715(13)	0.01785(15)	0.01825(14)	0.01737(13)
RE in 4*h* (*x*, *y*, ½)				
x	0.11888(3)	0.11884(4)	0.11859(3)	0.11828(3)
y	0.14360(3)	0.14306(3)	0.14280(3)	0.14265(3)
U_{eq}	0.01111(9)	0.01228(11)	0.01274(9)	0.01186(10)
In in 4*g* (*x*, *y*, 0)				
x	0.28787(4)	0.28925(5)	0.29017(4)	0.29083(4)
y	0.37759(3)	0.37649(4)	0.37587(4)	0.37542(3)
U_{eq}	0.01363(11)	0.01501(13)	0.01475(11)	0.01297(11)
S1 in 4*h* (*x*, *y*, ½)				
x	0.35795(13)	0.36016(17)	0.36144(16)	0.36283(14)
y	0.28606(12)	0.28423(16)	0.28313(14)	0.28200(13)
U_{eq}	0.0138(3)	0.0157(3)	0.0161(3)	0.0144(3)
S2 in 4*g* (*x*, *y*, 0)				
x	0.08293(12)	0.08445(16)	0.08519(15)	0.08574(13)
y	0.30578(11)	0.30450(14)	0.30338(13)	0.30275(12)
U_{eq}	0.0123(3)	0.0133(3)	0.0136(3)	0.0119(3)
S3 in 4*g* (*x*, *y*, 0)				
x	0.28700(12)	0.28563(15)	0.28456(14)	0.28383(12)
y	0.06262(11)	0.06262(14)	0.06234(13)	0.06236(12)
U_{eq}	0.0123(3)	0.0131(3)	0.0132(3)	0.0125(3)
S4 in 2*a* (0, 0, 0)				
U_{eq}	0.0134(4)	0.0155(5)	0.0148(4)	0.0134(4)

	$BaLa_2In_2Se_7$	$BaCe_2In_2Se_7$	$BaPr_2In_2Se_7$	$BaNd_2In_2Se_7$
Ba in 2*d* (0, ½, ½)				
U_{eq}	0.01872(13)	0.01983(14)	0.02140(18)	0.0226(2)
RE in 4*h* (*x*, *y*, ½)				
x	0.11764(3)	0.11734(3)	0.11675(4)	0.11659(5)
y	0.14234(3)	0.14183(3)	0.14146(4)	0.14121(4)
U_{eq}	0.01258(10)	0.01350(10)	0.01438(12)	0.01612(14)
In in 4*g* (*x*, *y*, 0)				
x	0.28359(4)	0.28480(4)	0.28528(5)	0.28615(6)
y	0.37792(4)	0.37729(4)	0.37700(5)	0.37645(6)
U_{eq}	0.01523(11)	0.01579(11)	0.01570(14)	0.01717(17)
Se1 in 4*h* (*x*, *y*, ½)				
x	0.35742(6)	0.35925(6)	0.36031(8)	0.36180(9)
y	0.28372(5)	0.28261(5)	0.28194(7)	0.28109(8)
U_{eq}	0.01423(14)	0.01563(14)	0.01607(18)	0.0180(2)
Se2 in 4*g* (*x*, *y*, 0)				
x	0.07792(5)	0.07923(5)	0.07991(7)	0.08085(9)
y	0.30564(5)	0.30446(5)	0.30361(7)	0.30288(8)
U_{eq}	0.01326(14)	0.01393(14)	0.01423(18)	0.0155(2)
Se3 in 4*g* (*x*, *y*, 0)				
x	0.28859(5)	0.28731(5)	0.28621(7)	0.28535(9)
y	0.06481(5)	0.06478(5)	0.06491(7)	0.06494(8)
U_{eq}	0.01331(14)	0.01417(14)	0.01464(17)	0.0161(2)
Se4 in 2*a* (0, 0, 0)				
U_{eq}	0.01340(18)	0.01467(18)	0.0147(2)	0.0164(3)

Table 3 Interatomic distances (Å) for Ba$RE_2In_2Ch_7$ (*RE* = La–Nd; *Ch* = S, Se)

	$BaLa_2In_2S_7$	$BaCe_2In_2S_7$	$BaPr_2In_2S_7$	$BaNd_2In_2S_7$
Ba–S3 (×4)	3.2986(11)	3.2952(14)	3.2968(13)	3.2971(12)
Ba–S2 (×4)	3.2997(11)	3.2963(14)	3.2998(13)	3.2984(12)
RE–S2 (×2)	2.8933(10)	2.8659(13)	2.8474(12)	2.8330(11)
RE–S3 (×2)	2.9955(10)	2.9679(13)	2.9541(12)	2.9431(11)
RE–S4 (×2)	3.0384(3)	3.0167(3)	3.0047(3)	2.9939(3)
RE–S1	3.1579(16)	3.131(2)	3.1175(19)	3.1022(17)
RE–S1	3.2956(16)	3.296(2)	3.3039(19)	3.3122(17)
In–S3	2.4576(15)	2.4562(19)	2.4558(17)	2.4568(16)
In–S1 (×2)	2.4689(9)	2.4609(12)	2.4558(11)	2.4540(10)
In–S2	2.5449(15)	2.5355(19)	2.5385(17)	2.5394(16)
In–S4	2.8979(5)	2.8801(6)	2.8734(5)	2.8679(5)
	$BaLa_2In_2Se_7$	$BaCe_2In_2Se_7$	$BaPr_2In_2Se_7$	$BaNd_2In_2Se_7$
Ba–Se2 (×4)	3.4089(5)	3.4112(5)	3.4139(7)	3.4142(9)
Ba–Se3 (×4)	3.4213(5)	3.4229(5)	3.4284(7)	3.4292(9)
RE–Se2 (×2)	3.0164(6)	2.9943(6)	2.9795(7)	2.9635(9)
RE–Se3 (×2)	3.1183(6)	3.0980(6)	3.0857(7)	3.0712(9)
RE–Se4 (×2)	3.1364(3)	3.1189(3)	3.1056(4)	3.0939(5)
RE–Se1	3.3036(8)	3.2802(8)	3.2666(11)	3.2493(13)
RE–Se1	3.4402(8)	3.4517(8)	3.4672(11)	3.4767(13)
In–Se3	2.5720(8)	2.5708(8)	2.5712(11)	2.5731(13)
In–Se1 (×2)	2.5870(5)	2.5811(5)	2.5777(6)	2.5732(8)
In–Se2	2.6684(8)	2.6657(8)	2.6670(11)	2.6648(13)
In–Se4	3.0675(5)	3.0536(5)	3.0509(7)	3.0424(8)

Table 4 Bond valence sums for Ba$RE_2In_2Ch_7$ (*RE* = La–Nd; *Ch* = S, Se)

	$BaLa_2In_2S_7$	$BaCe_2In_2S_7$	$BaPr_2In_2S_7$	$BaNd_2In_2S_7$
Ba	1.91	1.93	1.92	1.92
RE	2.87	2.91	2.86	2.87
In	3.10	3.16	3.18	3.19
S1	1.91	2.02	1.94	1.94
S2	2.09	2.13	2.12	2.13
S3	2.01	2.04	2.02	2.02
S4	1.83	1.86	1.84	1.85
	$BaLa_2In_2Se_7$	$BaCe_2In_2Se_7$	$BaPr_2In_2Se_7$	$BaNd_2In_2Se_7$
Ba	1.88	1.87	1.85	1.85
RE	2.72	2.86	2.80	2.83
In	3.00	3.04	3.05	3.07
Se1	1.83	1.86	1.86	1.87
Se2	2.01	2.07	2.05	2.07
Se3	1.94	1.98	1.96	1.96
Se4	1.77	1.85	1.83	1.84

Figure captions

Fig. 1. Plot of unit cell volumes for Ba$RE_2In_2Ch_7$ (RE = La–Nd; Ch = S, Se).

Fig. 2. (a) Structure of Ba$RE_2In_2Ch_7$ (RE = La–Nd; Ch = S, Se) viewed down the c-direction with one of the [In_2Ch_7] ribbons highlighted in polyhedral representation. (b) [In_2Ch_7] ribbon consisting of a double chain of corner-sharing InCh_5 trigonal bipyramids.

Fig. 3. Coordination polyhedra in Ba$RE_2In_2Ch_7$: (a) Ba in cubes (CN8), (b) RE in bicapped trigonal prisms (CN8), and (c) In in trigonal bipyramids (CN5).

Fig. 4. (a) Density of states (DOS) and (b) crystal orbital Hamilton population (–COHP) curves for $BaLa_2In_2S_7$.

Fig. 5. Optical spectra for $BaLa_2In_2S_7$ and $BaLa_2In_2Se_7$.

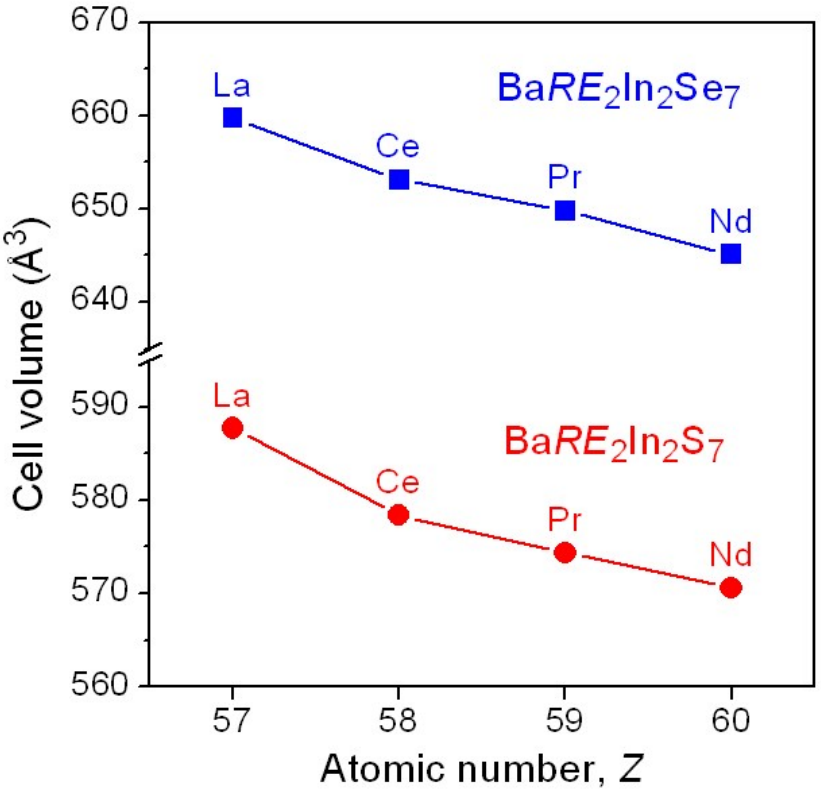

Fig. 1. Plot of unit cell volumes for BaRE_2In$_2Ch_7$ (RE = La–Nd; Ch = S, Se).

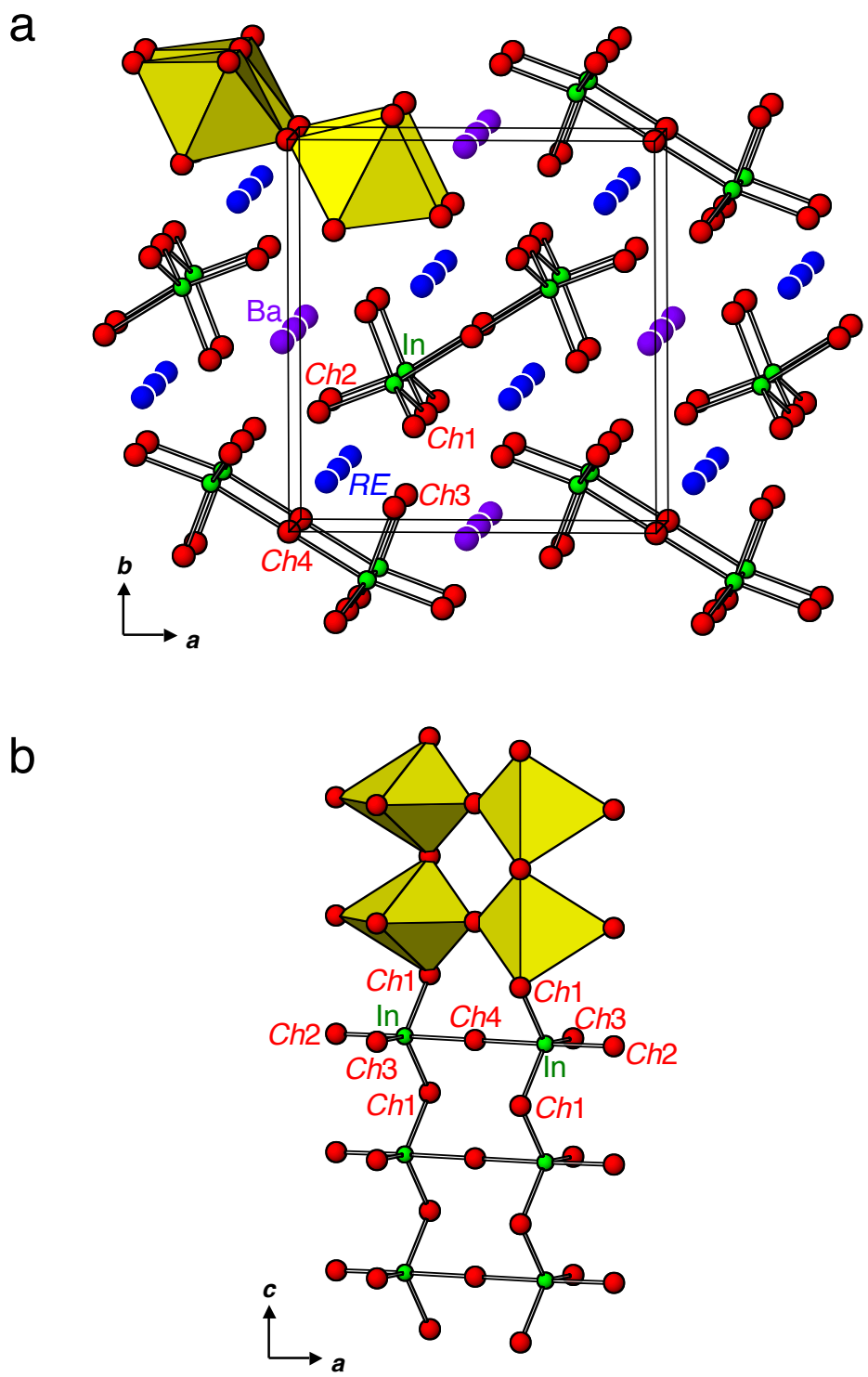

Fig. 2. (a) Structure of BaRE_2In$_2Ch_7$ (RE = La–Nd; Ch = S, Se) viewed down the c-direction with one of the [In$_2Ch_7$] ribbons highlighted in polyhedral representation. (b) [In$_2Ch_7$] ribbon consisting of a double chain of corner-sharing InCh_5 trigonal bipyramids.

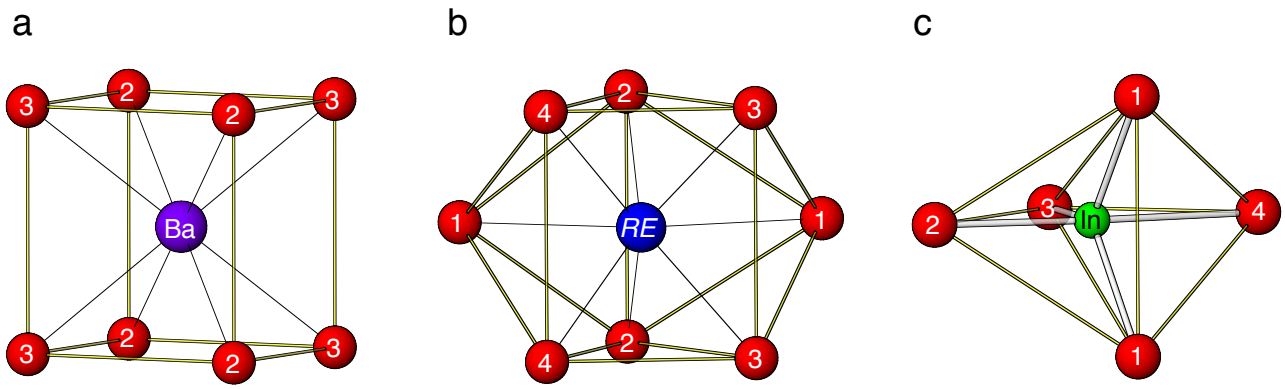

Fig. 3. Coordination polyhedra in BaRE_2In$_2$$Ch_7$: (a) Ba in cubes (CN8), (b) *RE* in bicapped trigonal prisms (CN8), and (c) In in trigonal bipyramids (CN5).

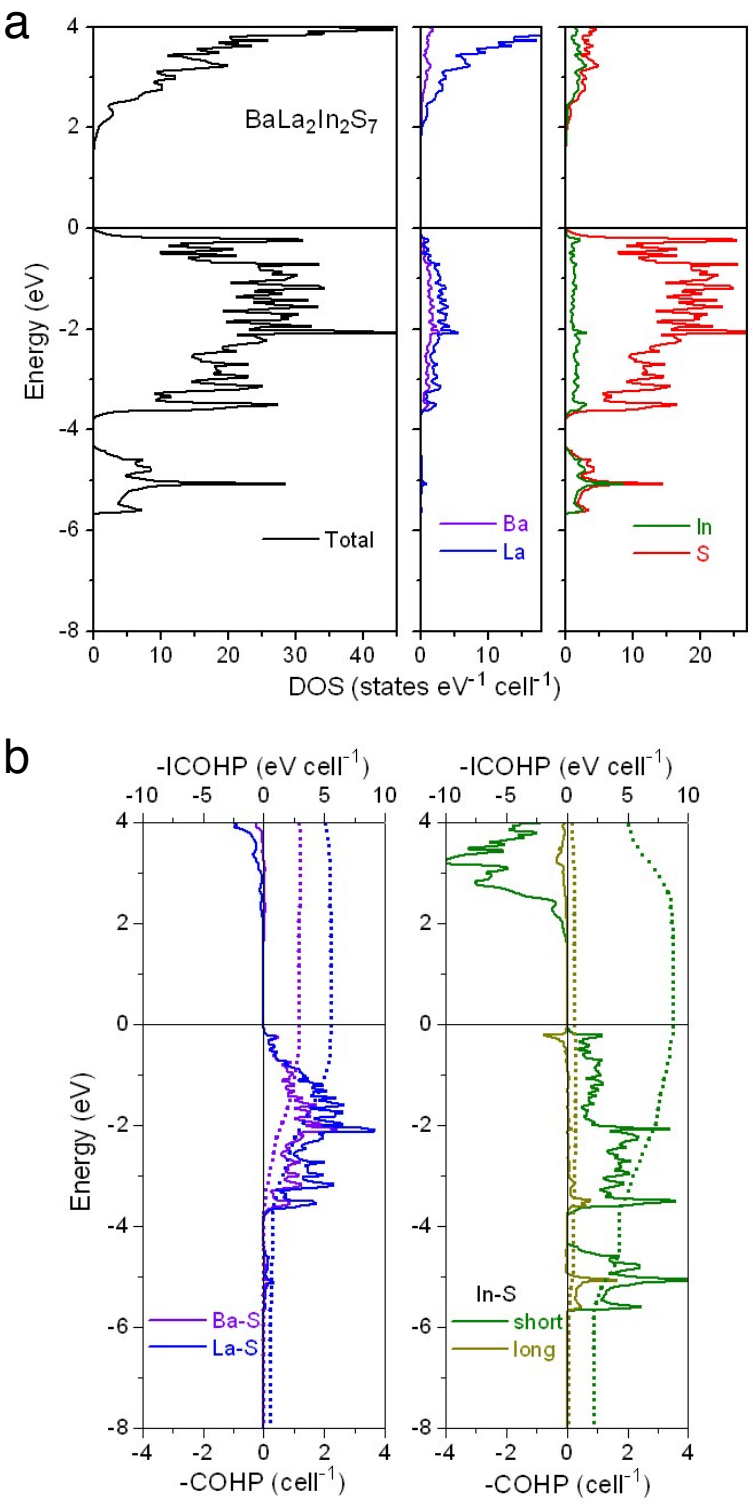

Fig. 4. (a) Density of states (DOS) and (b) crystal orbital Hamilton population (–COHP) curves for $BaLa_2In_2S_7$.

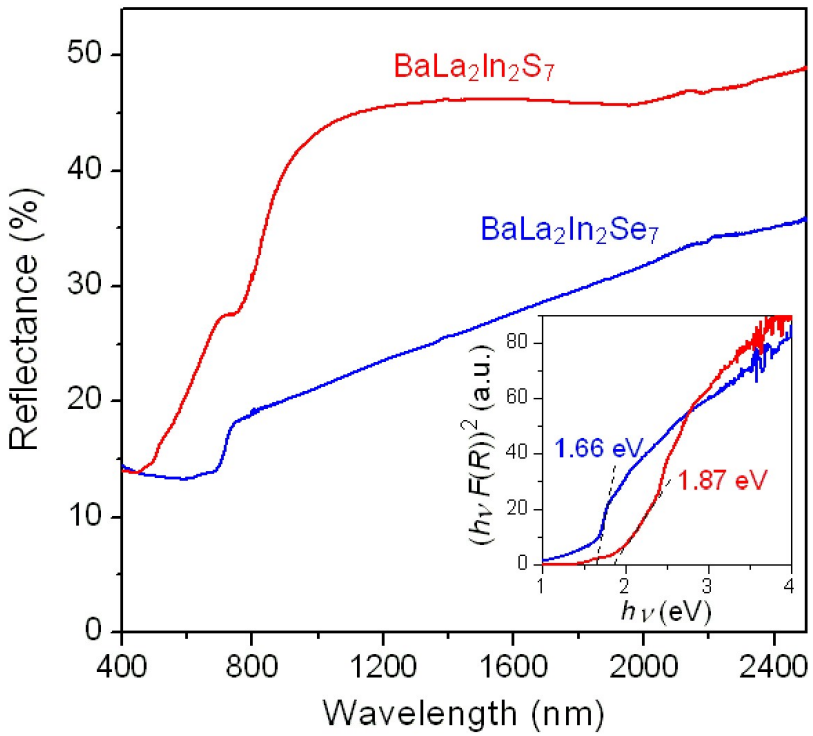

Fig. 5. Optical spectra for $BaLa_2In_2S_7$ and $BaLa_2In_2Se_7$.